JOURNAL OF SOLID STATE CHEMISTRY **139,** 388–397 (1998)
ARTICLE NO. SC987868

The Synthesis and Properties of the Chemically Oxidized Perovskite, $La_{1-x}Sr_xCoO_{3-\delta}$ ($0.5 \leq x \leq 0.9$)

Joseph E. Sunstrom IV, K. V. Ramanujachary, and Martha Greenblatt

Department of Chemistry, Rutgers, The State University of New Jersey, Piscataway, New Jersy 08854-8087

and

Mark Croft

Department of Physics, Rutgers, The State University of New Jersey, Piscataway, New Jersy 08854-8019

Received October 7, 1997; in revised form April 23, 1998; accepted April 28, 1998

The series of $La_{1-x}Sr_xCoO_{3-\delta}$ ($0.5 \leq x \leq 0.9$) perovskites have been prepared using the Pechini gel technique. The products were chemically oxidized by stirring in a sodium hypobromite solution. The samples have been characterized by powder X-ray diffraction, thermal analysis, iodometric titration, Co K edge X-ray absorption spectroscopy, temperature-dependent SQUID magnetic susceptibility, and temperature-dependent electrical resistivity. The Sr-rich samples ($x > 0.7$) have the brownmillerite-type structure prior to oxidation and the cubic perovskite structure after treatment with sodium hypobromite. Iodometric titration shows as much as a $\sim$14% increase in Co(IV) concentration in the Sr-rich samples after chemical oxidation. The Co K edge spectra show that there is very little change in the formal cobalt valence with increasing Sr content. The effective magnetic moments of the oxidized compounds level off with increasing Sr concentration. All of the chemically oxidized samples exhibit small-bandgap semiconducting behavior. The data lead to the postulation of an equilibrium between Co(IV) and O^- in the series.

INTRODUCTION

There has been a resurgence in research conducted on mixed-valent metal oxides adopting perovskitic structures within the last decade. To a large extent, this can be attributed to the recent discoveries of important phenomena such as high T_c superconductivity and colossal magnetoresistance in the pre-existing compounds $La_{2-x}Sr_xCuO_4$ (1) and $La_{1-x}Sr_xMnO_3$ (2, 3), respectively. Most of the current interest has been directed at mixed-valent first-row transition-metal oxides. Rare-earth cobaltates are one class of compounds which have potential for interesting magnetic and transport properties due to the availability of different oxidation and spin states. The combination of mixed valency with high/low spin states results in unique properties. One example is $LaCoO_3$, which is a perovskite with a rhombohedral unit cell that exhibits a thermally induced low-to-high spin transition resulting in an insulator-metal transition (4–24).

$La_{1-x}Sr_xCoO_3$, which exhibits metallic and ferromagnetic behavior, has been studied extensively (25–37). Most recently, $La_{1-x}Sr_xCoO_3$ ($0.0 < x \leq 0.3$) was reported to exhibit giant magnetoresistance at low temperatures (38–40). Most studies, however, have been conducted on the La-rich compositions ($x \leq 0.5$). The reasons for the previous investigations of the La-rich phases of $La_{1-x}Sr_xCoO_3$ were twofold and concerned both the cobalt valence and the crystal structure: it has been noted in several studies that it is difficult to stabilize more than approximately 50% Co(IV) in the series; in addition, at high ($x > 0.7$) Sr content, the compound crystallizes in a brownmillerite-like structure.

The other "end member" of the perovskite series, $SrCoO_3$, cannot be prepared in ambient or flowing oxygen conditions. Instead, the compound loses oxygen to retain low spin Co(III) and forms $Sr_2Co_2O_5$ which has the brownmillerite structure. Initial synthesis of $SrCoO_3$ was achieved at high ($\gg$150 MPa) oxygen pressures (32, 41–43). Recently, it has been shown that $Sr_2Co_2O_5$ can be oxidized to $SrCoO_3$ anodically in KOH solution (44–45). The brownmillerite $Sr_2Co_2O_5$ is a paramagnetic semiconductor while the perovskite $SrCoO_3$ is a ferromagnetic metal ($T_c =$ 280 K) (44).

Nemudry *et al.* showed that it is possible to oxidize $Sr_2Co_2O_5$ to $SrCoO_3$ by chemical oxidation (45). The chemical oxidation technique, or low-temperature oxygen intercalation, involves stirring a compound in a solution of sodium hypohalite at or below room temperature.

0022-4596/98 $25.00

This paper details the synthesis and characterization of $La_{1-x}Sr_xCoO_{3-\delta}$ ($0.5 \leq x \leq 0.9$) with the perovskite structure, which have been prepared by chemical oxidation.

EXPERIMENTAL

Synthesis. All chemicals were purchased at a minimum of reagent grade purity. La_2O_3 (Cerac, 99.99%) was heat treated at 1000°C for 24 h prior to use. $Co(NO_3)_2 \cdot 6H_2O$ (Fisher, 99.9%) and $Sr(NO_3)_2$ (BDH Chemicals, 99.5%) were verified for molecular weight by TGA. All samples used in this study were prepared by a gel-precursor technique. Lanthanum oxide La_2O_3 was dissolved in concentrated nitric acid. The subsequent $La(NO_3)_3$ solution was mixed with $Sr(NO_3)_2$ and $Co(NO_3)_2 \cdot 6H_2O$ in an aqueous solution. The stoichiometric aqueous metal nitrate solution was mixed with excess citric acid and ethylenediammine. The solution was heated to 100–120°C for 2–3 h to remove water and cause gel formation. The gel was slowly heated up to 600°C to decompose the nitrate salts and carbon precursors. The resultant ash was pressed into pellets and fired at 1100°C to complete the reaction. All products were gray-black.

Chemical oxidation. After the products were checked for phase purity by X-ray diffraction, approximately 0.5–0.7 g of sample was stirred into 100 ml of 5 M NaOH cooled in an ice bath. A 2.5–3.0 ml portion of Br_2 (Aldrich) was then added to the solution slowly. The resulting slurry was allowed to stir vigorously for 12–16 h at 4°C. The slurry was filtered, and the filtrate was washed several times with water and acetone. The filtrate was vacuum dried at room temperature. All products had a golden metallic color.

Thermal analysis. Thermogravimetric analysis (TGA) data was obtained using a TA Instruments Model 2050 thermogravimetric analyzer. Approximately 10–15 mg of sample was placed on a platinum pan and heated to 950°C at 10°C/min in flowing N_2 or O_2 (50 cc/min).

Iodometric titration. Average formal cobalt valence, and hence the total oxygen content was determined using a standard iodometric technique. Approximately 50 mg of sample and excess KI (iodate free) were stirred in 25 ml of water; concentrated hydrochloric acid was then added dropwise until the dissolution of all solids. Several drops of starch indicator were added to the samples giving the samples a dark-blue color. The samples were then titrated to a yellow-clear endpoint using a standard thiosulfate solution (Aldrich). All titrations were carried out under a blanket of argon.

Co K edge X-ray absorption spectroscopy (XAS). The Co K edge XAS measurements were performed on beam line X-19A at the Brookhaven National Synchrotron Light Source using a double crystal Si(311) monochromater. Electron yield, fluorescence mode (46, 47), and transmission mode measurements were made and all checked for consistency. A CoO standard was run simultaneously with all measurements for precise calibration. The relative energies between various spectra were established by careful comparison of the standard spectra. All spectra were normalized to unity step in the absorption coefficient from well below to well above the edge.

Structure. Powder X-ray diffraction data were measured using a Scintag PAD V diffractometer utilizing Cu$K\alpha$ radiation and a Li-drifted germanium detector. Samples were ground with silicon as an internal standard (NBS-681302) and placed on a glass slide with petroleum jelly. Lattice parameters were obtained independently by a non-linear least-squares fit and also by Rietveld refinement (48, 49) with the program GSAS (50).

Magnetic properties. Temperature-dependent magnetic susceptibility, (χ) measurements were made with a Quantum Design SQUID magnetometer (MPMS). The χ of the samples were measured from 10-350 K in an applied field of 1000 gauss.

Electrical properties. Temperature-dependent electrical resistivity, (ρ) measurements were carried out with a standard four-probe technique in a closed-cycle helium refrigerator (APD Cryogenics). Platinum leads were attached to the polycrystalline sample using a conducting silver epoxy.

RESULTS

Iodometric titration. The cobalt valences as determined by iodometric titration are shown in Table 1. (The oxidation states given in Roman numerals define low-spin (LS) and those given in Arabic numerals define high-spin (HS) electronic configurations hereafter.) Note that the iodometric titration gives the total number of highly oxidized species present, but does not confirm the identity of the oxidized

TABLE 1
Cobalt Valence in $La_{1-x}Sr_xCoO_{3-\delta}$ as Determined by Iodometric Titration[a]

	Atom percent Co(IV)	
x	"as prepared"	"chemically oxidized"
0.9	61.1 ± 0.6	68.4 ± 1.1
0.8	59.7 ± 0.5	73.5 ± 1.5
0.7	67.3 ± 0.2	67.9 ± 1.1
0.6	58.4 ± 0.2	60.2 ± 1.3
0.5	49.7 ± 0.1	50.3 ± 0.6

[a]Average and standard deviation based on 5 titrations.

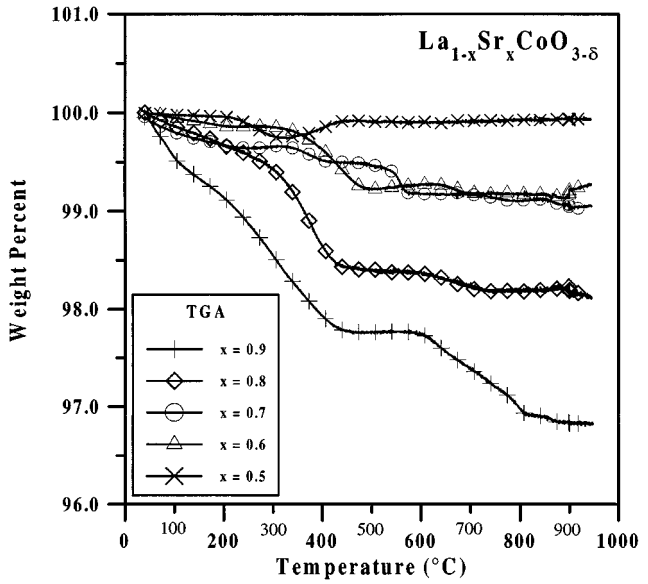

FIG. 1. Difference thermal analysis profiles for $La_{1-x}Sr_xCoO_{3-\delta}$. This graph is the TGA of the "as prepared" samples subtracted from the chemically oxidized samples.

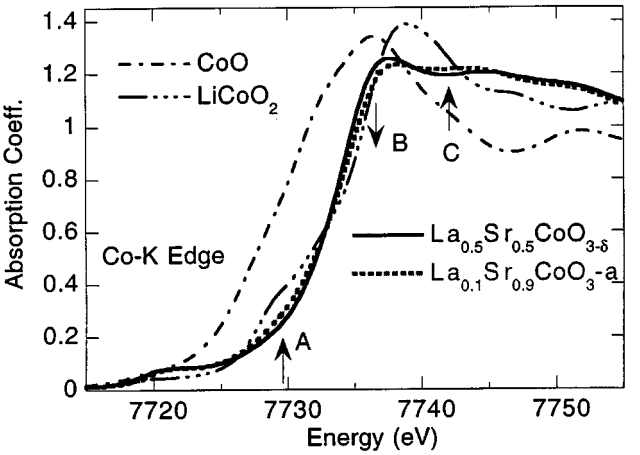

FIG. 2. Co K edge XAS for CoO, $LiCoO_2$, and chemically oxidized $La_{0.1}Sr_{0.9}CoO_{3-\delta}$ and as prepared $La_{0.5}Sr_{0.5}CoO_{3-\delta}$.

species. For ease of comparison, it is assumed that all of the iodide oxidation is due to Co(IV). It will be shown later that this may not be an appropriate assumption.

Thermal analysis. Figure 1 shows the difference traces of the TGA data for the "as prepared" samples subtracted from the TGA data for the chemically oxidized samples. The TGA experiments were run under nitrogen with identical gas flow rates and ramp sequences. Quantitative information cannot be determined from the TGA results, due to the inability to correctly identify the compositions of the end products. However, some qualitative comparisons can be made from the data.

Co K edge XAS. A comparison of the Co K edge spectra of the formally Co^{2+}/Co(III) compounds, $CoO/LiCoO_2$, is shown in Fig. 2. Note the strong chemical shift between these materials consistent with a formal valence increase involving strong Co *d* hole creation. Also included in the figure are the spectra for two $La_{1-x}Sr_xCoO_{3-\delta}$ perovskite-compounds: that of the $x = 0.9$, after oxidation (hereafter denoted as "-a") material and that of the $x = 0.5$ material. While the perovskite compounds exhibit less structure on the steeply rising portion of the edge, it is clear that the centrum of their edges lies close to that of $LiCoO_2$ and to each other. This supports the notion that the Sr substitution-induced holes have little Co *d* character. The opposite case is well illustrated, by recent work from this group, on the $La_{1-x}Ca_xMnO_3$ system, where the chemical shifts and d-hole character are both large (51).

In Figs. 2 and 3, the labels A, B, and C identify the energy ranges of features that are tentatively assigned here to Co 4*p* features. The intensity transfer between these features can be associated with modest decreases in *d* orbital occupancy.

A comparison of titration (inset) and the Co K edge results on the $La_{1-x}Sr_xCoO_{3-\delta}$ system before (-b) and after (-a) oxidation is shown in Fig. 3. The inset shows the percentage of formal Co(IV), as determined by iodometric titration of this system, as a function of Sr content.

Structure. Figures 4 and 5 show the X-ray diffraction patterns for the series $La_{1-x}Sr_xCoO_{3-\delta}$ ($0.5 \le x \le 0.9$) before and after chemical oxidation, respectively. The X-ray

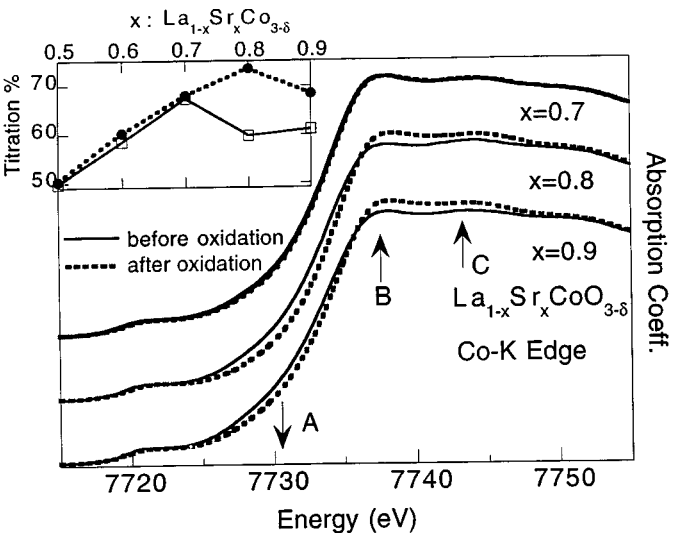

FIG 3. Co K edge XAS for "as prepared" $La_{0.1}Sr_{0.9}CoO_{3-\delta}$ and chemically oxidized $La_{0.1}Sr_{0.9}CoO_{3-\delta}$. The inset shows the percentage of formal Co(IV) as determined by iodometric titration on the "as prepared" and chemically oxidized $La_{1-x}Sr_xCoO_{3-\delta}$ ($0.5 \le x \le 0.9$).

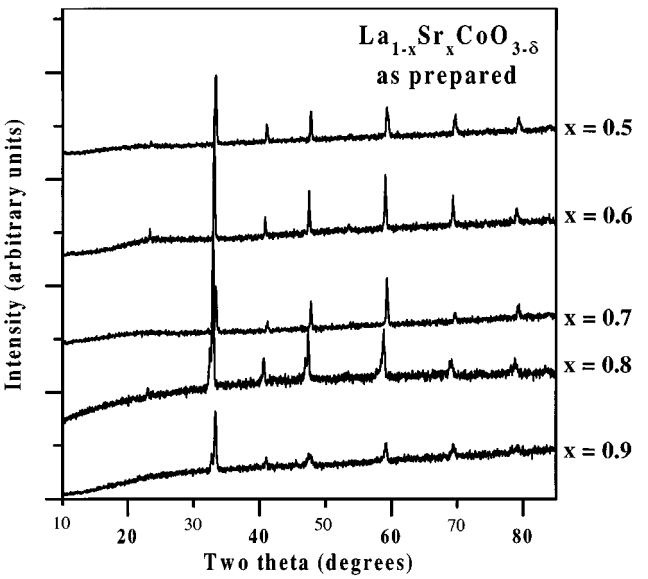

FIG. 4. X-ray diffraction patterns for the "as prepared" samples (from bottom to top) $La_{0.1}Sr_{0.9}CoO_{3-\delta}$, $La_{0.2}Sr_{0.8}CoO_{3-\delta}$, $La_{0.3}Sr_{0.7}CoO_{3-\delta}$, $La_{0.4}Sr_{0.6}CoO_{3-\delta}$, and $La_{0.5}Sr_{0.5}CoO_{3-\delta}$.

diffraction patterns for the "as prepared" $La_{1-x}Sr_xCoO_{3-\delta}$ samples show that the perovskite structure is retained when $x \leq 0.7$, then transforms to a brownmillerite-type structure at higher concentrations of Sr doping. The structure change is manifested in a splitting/broadening of the peaks. Figure 5 shows that it is possible to synthesize single-phase perovskite across the studied series by chemical oxidation.

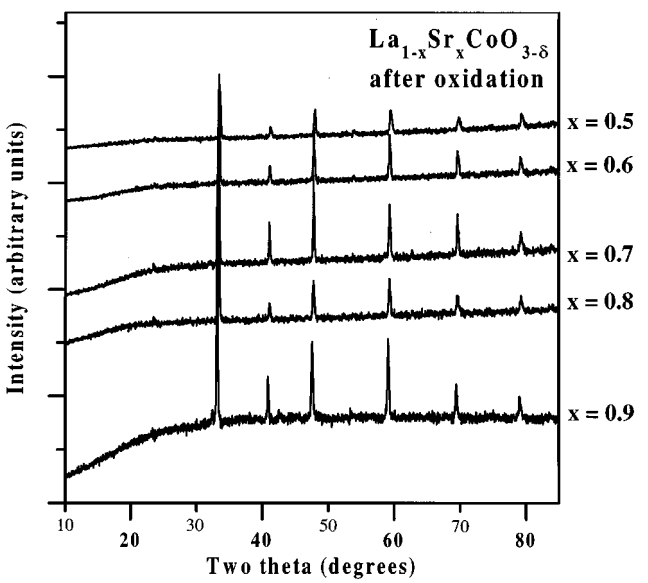

FIG. 5. X-ray diffraction patterns for the chemically oxidized samples (from bottom to top) $La_{0.1}Sr_{0.9}CoO_{3-\delta}$, $La_{0.2}Sr_{0.8}CoO_{3-\delta}$, $La_{0.3}Sr_{0.7}CoO_{3-\delta}$, $La_{0.4}Sr_{0.6}CoO_{3-\delta}$, and $La_{0.5}Sr_{0.5}CoO_{3-\delta}$.

TABLE 2
Lattice Parameters and *M*–O Distances for "as Prepared" $La_{1-x}Sr_xCoO_{3-\delta}$

x	a_0 (Å)	Co–O distance (Å)	La/Sr–O distance (Å)
0.7	3.800(3)	1.900(1)	2.687(3)
0.6	3.823(2)	1.911(1)	2.703(1)
0.5	3.798(2)	1.899(1)	2.686(2)

Tables 2 and 3 give the lattice parameters and metal oxygen distances for the "as prepared" and chemically oxidized $La_{1-x}Sr_xCoO_{3-\delta}$ samples, respectively. The metal–oxygen distances have been calculated directly from the refined lattice parameters. The general trend for both the "as prepared" and chemically oxidized samples is that the lattice parameter and metal–oxygen distances increase with increasing Sr content.

Magnetic properties. Figures 6 and 7 show the molar magnetic susceptibility, χ_M, vs temperature (T) plots for the $La_{1-x}Sr_xCoO_{3-\delta}$ ($x = 0.9$, 0.8) samples before and after chemical oxidation.

Figure 8 shows the χ_M vs T plot for the $La_{0.5}Sr_{0.5}CoO_{3-\delta}$ sample before and after chemical oxidation and illustrates well that there is little change upon chemical oxidation. Figure 9 is a plot of μ_{eff} as a function of Sr content, x in $La_{1-x}Sr_xCoO_{3-\delta}$ before ($\times$) and after ($\blacklozenge$) chemical oxidation. For the "as prepared" samples μ_{eff} decreases from $x = 0.5$ to $x = 0.6$ in agreement with previous studies, which suggest that the maximum formal Co(IV) concentration exists at $x = 0.5$ (8).

Tables 4 and 5 give the results of Curie–Weiss fits for the "as prepared" and chemically oxidized samples, respectively. All samples are ferromagnetic. Large changes in Curie temperature, T_{Curie}, are apparent in the $La_{1-x}Sr_xCoO_{3-\delta}$, $x = 0.9$ and 0.8, samples which have the highest degree of chemical oxidation and a brownmillerite-like-to-perovskite structure change.

Electrical properties. Figure 10 shows the resistivity (ρ) vs T curves for the series of oxidized compounds. The room

TABLE 3
Lattice Parameters and *M*–O Distances for $La_{1-x}Sr_xCoO_{3-\delta}$ after Oxidation

x	a_0 (Å)	Co–O distance (Å)	La/Sr–O distance (Å)
0.9	3.825(1)	1.912(1)	2.705(1)
0.8	3.802(1)	1.901(1)	2.689(1)
0.7	3.802(1)	1.901(1)	2.689(1)
0.6	3.797(1)	1.899(1)	2.685(1)
0.5	3.784(1)	1.891(1)	2.675(1)

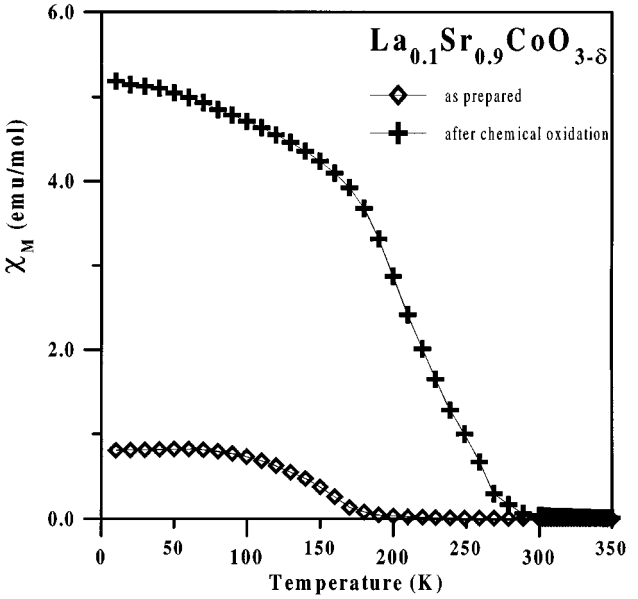

FIG. 6. Molar magnetic susceptibility as a function of temperature for $La_{0.1}Sr_{0.9}CoO_{3-\delta}$.

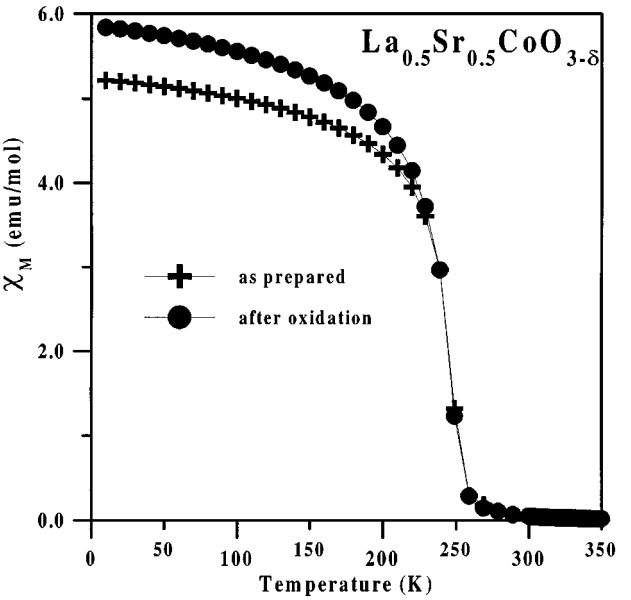

FIG. 8. Molar magnetic susceptibility as a function of temperature for $La_{0.5}Sr_{0.5}CoO_{3-\delta}$.

temperature resistivities for the chemically oxidized compounds are in the 1–10 Ω cm range. These ρ values are 2–3 orders of magnitude lower than the resistivities of the "as prepared" samples.

Figure 11 shows the $\ln(\rho)$ vs $1/T$ fits for the oxidized compounds in the 200–300 K range. The activation energies (E_a) are summarized in Table 6. The E_a values are small for the whole series, with the $x = 0.5$ sample having the lowest E_a (0.015 eV). The remaining samples have approximately the same activation energy with the exception of the $x = 0.9$ sample, which has a lower activation energy probably due to the fact that it is not fully oxygenated.

DISCUSSION

Synthesis. The Pechini gel method (52) allows greater homogeneity, smaller particle sizes and lower processing

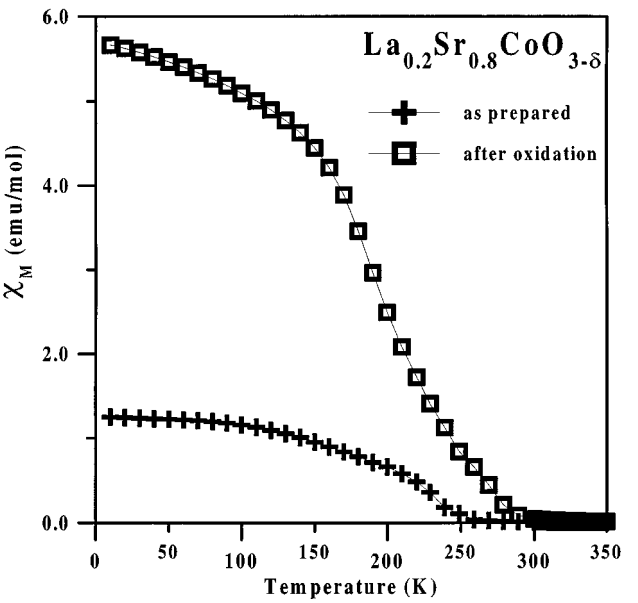

FIG. 7. Molar magnetic susceptibility as a function of temperature for $La_{0.2}Sr_{0.8}CoO_{3-\delta}$.

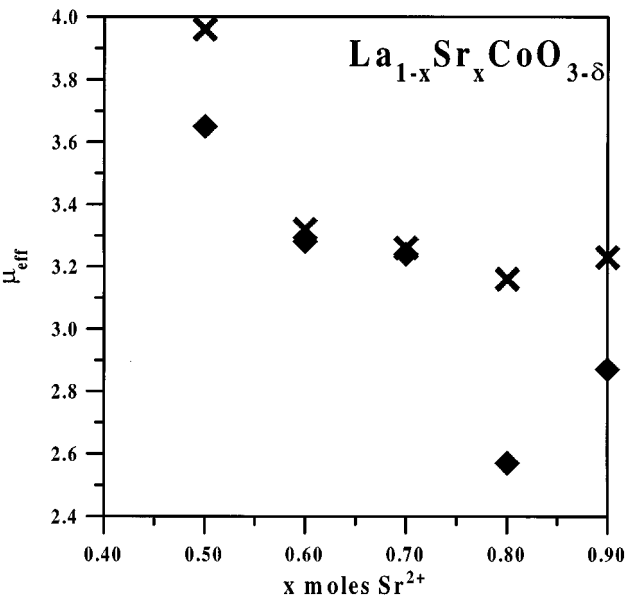

FIG. 9. Effective magnetic moment, μ_{eff}, as a function of Sr content in $La_{1-x}Sr_xCoO_{3-\delta}$ before (◆) and after (×) chemical oxidation.

TABLE 4
Curie–Weiss Parameters for "as Prepared" $La_{1-x}Sr_xCoO_{3-\delta}$

x	C (emu mol/K)	T_{Curie} (K)	μ_{eff} (BM)
0.9	1.04	170.4	2.87
0.8	0.833	226.9	2.57
0.7	1.31	244.6	3.24
0.6	1.34	220.4	3.28
0.5	1.67	267.4	3.65

temperatures than standard solid state reaction of oxides. The compounds in this study could be prepared as low as 800°C. Co-precipitation has similar benefits but has one disadvantage. The co-precipitation technique assumes that all metal ions precipitate completely and at the same rate. However, many combinations of metal ions do not precipitate at the same rate, which leads to errors in product stoichiometry. The Pechini method is one where the metal stoichiometry is retained throughout the process as long as the metals are nonvolatile.

Chemical oxidation. The chemical oxidation technique has been shown to be effective in the synthesis of other highly oxidized compounds (e.g., $La_2CuO_{4+\delta}$ (53) and $Ce_2Zr_2O_{7+\delta}$ (54)). Table 1 indicates that the "as prepared" compositions which crystallize in the perovskite structure ($x \leq 0.7$) are nearly fully oxidized and thus show very little change in valence after treatment with NaOBr. The two brownmillerite compositions ($x = 0.8$ and 0.9) show dramatic changes in the Co(IV) content after chemical treatment. One major disadvantage of chemical oxidation is the inability to control the degree of oxidation in the sample. Moreover, the mechanism of oxygen insertion in this process is not well understood.

Thermal analysis. The TGA graph (Fig. 1) clearly shows that oxygen loss or "thermal de-intercalation" is related to the strontium content. This can be easily explained on the basis of the charge of the A cation in the perovskite structure. The oxygens being removed are in the coordination sphere of the La/Sr cation. As the Sr content increases, the average effective charge of the A cation decreases due to

TABLE 5
Curie–Weiss Paramters for $La_{1-x}Sr_xCoO_{3-\delta}$ after Oxidation

x	C (emu mol/K)	T_{Curie} (K)	μ_{eff} (BM)
0.9	1.30	269.4	3.23
0.8	1.25	272.3	3.16
0.7	1.34	241.1	3.26
0.6	1.38	227.9	3.32
0.5	1.96	262.1	3.96

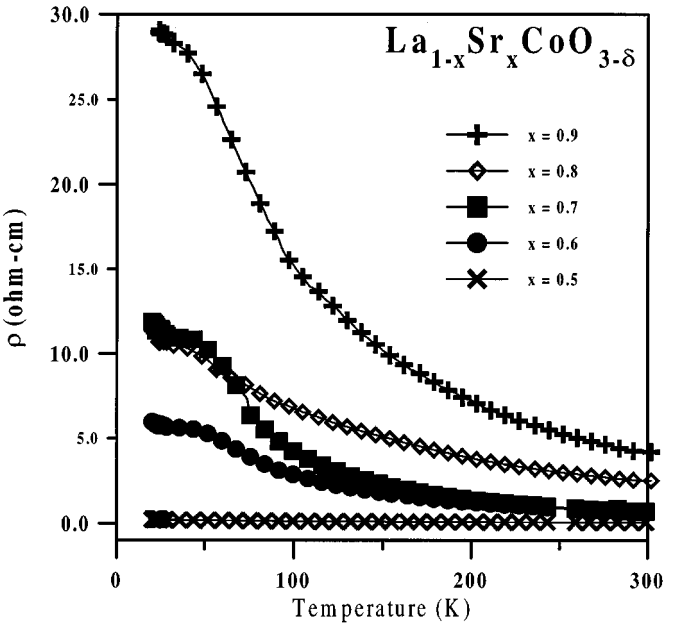

FIG. 10. Resistivity as a function of temperature for (from top to bottom) $La_{0.1}Sr_{0.9}CoO_{3-\delta}$ (+), $La_{0.2}Sr_{0.8}CoO_{3-\delta}$ (◇), $La_{0.3}Sr_{0.7}CoO_{3-\delta}$ (■), $La_{0.4}Sr_{0.6}CoO_{3-\delta}$ (●), and $La_{0.5}Sr_{0.5}CoO_{3-\delta}$ (×).

replacement of trivalent La with divalent Sr cations. The TGA data also provides additional evidence that the oxidant is chemically bound in the sample. The degree of oxygen de-intercalation is linked to the composition of the host lattice even though the extent of oxygen intercalation is variable and appears to be maximum at $x = 0.8$ (Table 1). It

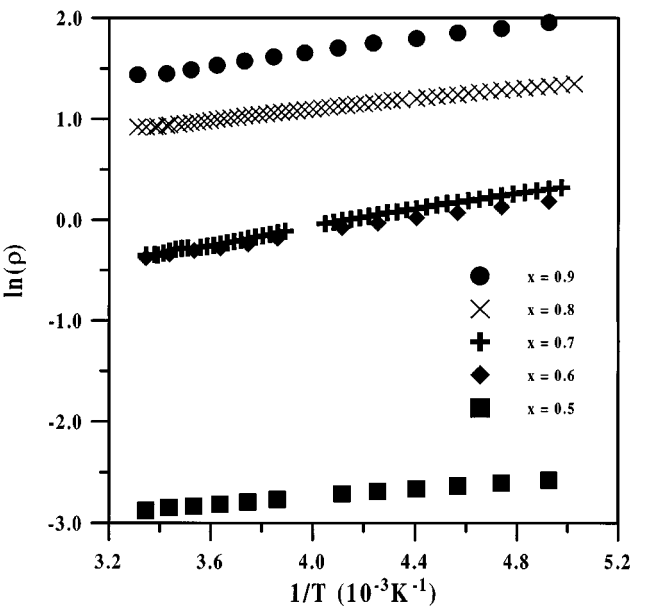

FIG. 11. Ln(ρ) vs $1/T$ fits for $La_{1-x}Sr_xCoO_{3-\delta}$.

TABLE 6
Activation Energies for Chemically Oxidized $La_{1-x}Sr_xCoO_{3-\delta}$

x	E_a (eV)
0.5	0.015
0.6	0.03
0.7	0.03
0.8	0.03
0.9	0.022

should also be noted that the oxidized compounds de-intercalate oxygen at fairly low temperatures (< 500 K). In fact, the $x = 0.9$ sample loses weight slowly even at room temperature. This may explain why the titration data indicates a lower degree of oxidation for the $x = 0.9$ sample when compared to the $x = 0.8$ sample. Finally, the relative low thermal stability of the compounds precludes their sintering.

Co K edge XAS. The near K-edge features of 3*d* transition metal (*T*) compounds are typically interpreted in terms of transitions into *T*–4*p* final states with differing *T*–3*d*/ligandhole configurations. The ground state of the transition metal–ligand cluster in such compounds will involve a superposition of several *d*-state configurations, such as the d^6–$d^7\underline{L}$–$d^8\underline{L}_2$ (here the $\underline{L}$ refers to a hybridized ligand hole) state admixture proposed for $LaCoO_3$ (55–57). A formal *T* valence increase in such compounds involves a shifting of the quantum mechanical weight from higher to lower *d* occupancy configurations. In the *T* K edge spectra such a *T* valence increase is associated with the transfer of intensity from the lower energy features (with higher *d* electron count) to the higher energy features (with lower *d* electron count). Here the attractive Coulomb interaction energy between the *d*-electrons and the photo-induced core hole moves the higher *d* electron count features closer to the edge.

The direction of the arrows in Fig. 2 indicate the spectral intensity change between the $x = 0.5$ and the $x = 0.9$ -a spectra. Thus the decrease of B feature intensity and the modest increase of C feature intensity, upon Sr substitution, is consistent with a modest *d*-hole increase (i.e. the shift in weight from higher to lower *d*-occupancy states hybridized into the ground state). However, there is also a small A feature intensity increase between $x = 0.5$ and the $x = 0.9$ -a spectra, indicating that a higher *d* count configuration could be somewhat stabilized upon Sr substitution. This gain, albeit modest, in the intensity of the A feature, with increasing overall formal transition metal valence, is quite unusual and can be clarified when the effect of oxidation treatment of these materials is considered below.

With the exception of the "before" $x = 0.8$ and 0.9 materials, which have a brownmillerite-like structure, all of the other compounds are single phase perovskite structure. The changes in the Co K edge spectra before and after oxidation are clear for the 0.8 and 0.9 materials, almost imperceptible for $x = 0.7$ and lower compositions not shown in Fig. 3. The effect of the oxidation in the $x = 0.8$ and 0.9 spectra is to decrease the A feature intensity while enhancing both the B and C features (the arrows in the figure near each of the features point to the amplitude changes of the features upon oxidation). This spectral weight transfer is consistent with the transfer of weight from lower to higher *d* hole contributions to the hybridized Co ground state.

The iodometric titration (inset Fig. 3) and XAS results are clearly in excellent agreement regarding the onset of the material's strong response to the oxidation treatment above $x = 0.7$. Indeed, the somewhat higher response in the titration result at $x = 0.8$ is subtly reflected in the XAS results also.

Thus the A feature is particularly strong in the brownmillerite-type structure, where Co sites with an O vacancy are arrayed in planes. Less Co-to-O charge transfer and a higher Co *d* count at these O-vacancy Co sites would be therefore expected in the brownmillerite-type material. The association of the A feature with these vacancy-induced high Co *d* count sites is consequently reasonable. Moreover, the substantial quenching of the A feature upon oxidation filling of these O vacancies (and conversion to the perovskite structure) underscores this interpretation.

Potze *et al.* have proposed an electronic configuration for perovskite $SrCoO_3$ which is dominated by a 67% $d^6\underline{L}$ configuration with 25% $d^7\underline{L}_2$ and 8% d^5 admixtures (58). For $LaCoO_3$, Saitoh *et al.* have discussed competing low (LS), intermediate (IS), and high spin (HS) configurations with varying weights of d^6, $d^7\underline{L}$, and $d^8\underline{L}_2$ admixtures (57). The configurations favored at lower temperatures are the LS and IS states which manifest a plurality of weight about 53% in the $d^7\underline{L}$ state followed by 29–35% in the d^6 state, and 12–17% in the $d^8\underline{L}_2$ state. Saitoh *et al.* emphasized the strongly hybridized Co *d*/O *p* character of this material and the considerable *p*-*p* character of the states on either side of the gap (57). The LDA + U (a combination of the local density approximation and Hubbard models) calculations of Korotin *et al.* on $LaCoO_3$ also underscored such hybridization produced Co *d* electron counts close to 7, and paraphrased their results in terms of a strong $d^7\underline{L}$ character (56). The molecular orbital calculations of Takahashi *et al.* on $LaCoO_3$ also yielded a strongly hybridized LS ground state (55). Moreover, they presented schematic density of states with filled O *p* states closest to the Fermi energy, E_F and therefore implying that O holes would be the dominant response mode to Sr^{2+} substitution. Indeed, Takahashi *et al.* emphasize the resemblance of the $La_{1-x}Sr_xCoO_3$ systems to the $La_{1-x}Sr_xCuO_{4-\delta}$ system (55).

To attempt to assign specific *d* configurations to the various Co K edge XAS features, one should recall that in the previous electronic structure work $LaCoO_3$ was

considered to be dominated by the mixed $d^7\underline{L}/d^6$ configurations and $SrCoO_3$ by the $d^6\underline{L}/d^7\underline{L}_2$ mixture (55–58). With this in mind, association of the most intense (B) feature in the $x = 0.5$ spectrum (Fig. 2 and in the $x = 0.0$ spectrum not displayed) with the d^6 configuration would appear most reasonable. The more subtle ligand hole states associated with the various d configurations will be suppressed for simplicity. Spectral intensity in the A region is then associated with the d^7 configuration and the C feature with the d^5 configuration. With this interpretation the Sr-induced transfer of intensity form the B to C features (in the purely perovskite structure materials) represents a shift from d^6 to d^5 weight in the hybridized ground state. Similarly, the presence of enhanced A intensity at the expense of the B–C intensity in the brownmillerite material spectrum would presumably be associated with the loss of d^6/d^5 character and gain of d^7 character due to O-deficient sites.

It must be emphasized that the d count changes evidenced by these XAS results, though discernible, are modest. The lack of significant chemical shifts at the Co K edge support the notion that the Sr-induced hole formation occurs predominantly in the O p orbitals with the Co d responses coming through hybridization.

It is worth noting that interpretation of the XAS features is reminiscent of Ni perovskite-based systems where a d^7 (Ni^{3+}) identification has proved consistent with a C-type feature similar to that identified with d^5 (Co(IV)) here. This is illustrated in Fig. 12, where the Ni K XAS spectra of a series of Ni perovskite-based structures with formal Ni valences varying from 2 to 3 are shown (60). The B feature

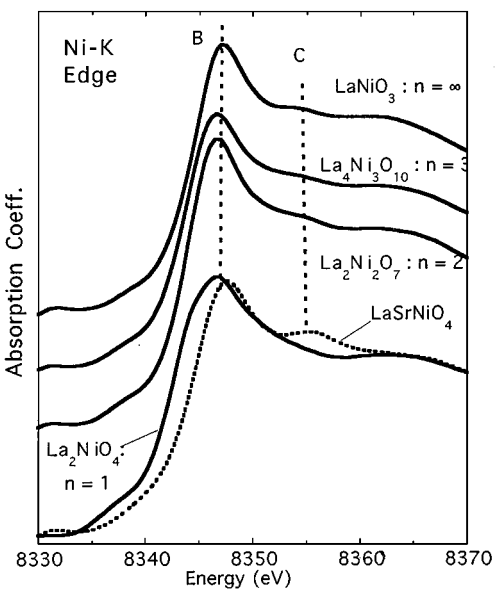

FIG. 12. Ni K edge XAS for a series of nickelates with different Ni^{3+} content: La_2NiO_4, $LaSrNiO_4$, $La_3Ni_2O_7$, $La_4Ni_3O_{10}$, and $LaNiO_3$ (after (Ref. (60)).

was associated with the d^8 configuration (again the ligand hole addendum is suppressed). In the formally divalent La_2NiO_4 material, the C feature is essentially absent; however, it is seen to grow systematically in intensity with increasing formal Ni valence until it is rather robust in the formally trivalent $LaSrNiO_4$ material. The fact that the B d^8 feature remains strong in even the trivalent compound reflects both the hybridized nature of the d configuration and the energetic difficulty of stabilizing a fully Ni^{3+}-pure-d^7 state (60).

Structure. The Shannon–Prewitt radii for Co(III) and Co^{4+} (0.685 and 0.67 Å for $CN = 6$) are similar (61). Note the effective ionic radius, r_{eff}, is only given for the HS state of tetravalent Co (Co^{4+}) in Ref. (61), but the r_{eff} of Co(III) and Co^{3+} (0.75 Å) are similar. By analogy it is assumed that r_{eff} of the LS and HS state of Co in the 4+ state will be also similar. Since the ratio Co(III)/Co(IV) and the nature of the oxygen species are unknown in $La_{1-x}Sr_xCoO_{3-\delta}$, it becomes difficult to rationalize the lattice parameters on the basis of the Co–O distances. In fact, the observed Co–O distances (1.89–1.91 Å) are shorter than the calculated distances of 1.945 and 1.93 Å for Co(III)–O^{2-} and Co(IV)–O^{2-}, respectively. The slight expansion of cell volume is most likely driven by the increasing average size of the A cation. The Shannon–Prewitt radii for Sr^{2+} and La^{3+} are 1.58 and 1.50 Å for $CN = 12$, respectively (61). Using a weighted average of these radii, the average radius of the A site goes from 1.54 to 1.57 Å for $x = 0.5$ to 0.9. This would account for the small expansion of cell volume.

Magnetic properties. High spin Co^{4+} has d^5 ($t_{2g}^3e_g^2$) spin configuration with $S = \frac{5}{2}$ and an effective magnetic moment, $\mu_{eff} = 5.92$ BM. Similarly, Co(IV) with d^5 ($t_{2g}^5e_g^0$) LS electronic configuration and $S = \frac{1}{2}$ would be expected to have $\mu_{eff} = 1.73$ BM. The experimentally observed values of μ_{eff} in Tables 4 and 5, as determined from a Curie–Weiss fit of the data in the high temperature (300–360 K) region are intermediate between the theoretical μ_{eff} for HS and LS electronic configurations of tetravalent Co. Similar values of μ_{eff} have been noted in the La-rich compositions ($0.0 \leq x \leq 0.5$) and were effectively explained with an intermediate spin configurational model (27). There is also a large decrease in the effective moment for the $x = 0.9$ and 0.8 "as prepared" samples (Table 4) due to the formation of oxygen vacancies which lower the average valence of the Co. The chemically oxidized series again show a relatively large decrease of μ_{eff} between the $x = 0.5$ and 0.6 samples. The μ_{eff} then levels to approximately the same value for the remaining compositions (Fig. 9). This finding is consistent with the equilibrium between Co(IV) and O^- which is discussed below. The largest change in μ_{eff} between "as prepared" and chemically oxidized samples occurs for the $x = 0.9$ and 0.8 compositions (Tables 4 and 5). Again, these compositions have the highest degree of oxidation as

evidenced by iodometric titration, and undergo a structural change upon oxidation.

The structural change in the oxidized $x = 0.8$ and 0.9 samples is also manifested by the dramatic increase of the Curie temperature and the magnitude of χ below the ferromagnetic transition as illustrated in Figs. 6 and 7. This result is due to the –Co–O–Co– bond angle approaching the ideal $\sim 180^\circ$ expected in the perovskite structure, thus enhancing the ferromagnetic exchange coupling. A similar effect of the perovskitic –Co–O–Co– $\sim 180^\circ$ interactions is evident in Fig. 8 by the large ferromagnetism of $La_{0.5}Sr_{0.5}CoO_{3-\delta}$.

Electrical properties. The resistivities were measured on pressed polycrystalline pellets which could not be sintered due to the thermal instability of the compounds. The lack of sintering is expected to increase the observed resistivities of the samples.

Considering that the titration data indicate that the number of oxidized species increases with increasing Sr content (Table 1), while the Co K edge XAS spectra show that the formal Co valence is not changing, it can be postulated that the following equilibrium exists:

$$\text{Co(IV)} + \text{O}^{2-} \leftrightarrow \text{Co(III)} + \text{O}^{-}. \qquad [1]$$

The equilibrium moves to the right at high Sr concentrations. The fact that highly electropositive metals like Sr stabilize peroxides makes this equilibrium even more plausible. The powder X-ray diffraction data is consistent with the formation of O^- anions. The radius of O^- should be smaller than that of O^{2-} and thus lead to shorter Co–O bonds. The Co–O bonds for the chemically oxidized series are generally shorter (Tables 2 and 3) than those for the "as prepared" samples, which agrees with a higher concentration of O^- anions in the former. Moreover, the "leveling" of the magnetic moment with increasing Sr content (Table 5, Fig. 9) is another indication that the Co(IV) concentration has reached a maximum and oxidation of the oxide ion is occurring. Finally, there is spectroscopic evidence that $LaCoO_3$ is a charge-transfer insulator with the O-2p band located immediately below the empty-*d* upper-Hubbard band (33). Thus the electronic band structure could facilitate the process indicated in Eq. [1].

Goodenough proposes a model based on hole rich and hole poor clusters for the series $La_{1-x}Sr_xCoO_{3-\delta}$ ($0.0 \leq x \leq 0.5$) (36). The model is based on the formation of clusters of Co(IV) ferromagnetically coupled with 6 (Co(III)/Co^{3+}) nearest neighbors (36). This cluster model combined with our data provides a good explanation why the maximum Co(IV) concentration is approximately at $x = 0.5$ in $La_{1-x}Sr_xCoO_{3-\delta}$: at $x = 0.5$, there would be 50% Co(IV) in the lattice which would be the maximum allowable to maintain the formation of Co(IV)–$(\text{Co(III)/Co}^{3+})_6$ clusters; at $x > 0.5$, there would be formally more than 50% Co(IV) present which would lead to Co(IV)–Co(IV) nearest-neighbor interactions. Our data suggest that, instead, the oxygen is oxidized allowing the structure to retain the Co(IV)–$(\text{Co(III)/Co}^{3+})_6$ nearest-neighbors. The introduction of the O^- into the Co(IV)–(Co(III)/Co^{3+}) linkage would also lead to an antiferromagnetic interaction causing a reduction of moment. This is consistent with our data in that the magnitude of the moment does not just level off at $x = 0.5$ and remain the same with increasing x, but experiences a small decrease at $x > 0.5$, then levels off with increasing x (see Fig. 9).

CONCLUSIONS

The series of $La_{1-x}Sr_xCoO_{3-\delta}$ ($0.5 \leq x \leq 0.9$) has been prepared using a citrate gel technique at relatively low temperature. The "as prepared" samples transform from the cubic-perovskite ($0.5 \leq x \leq 0.7$) to a brownmillerite-like structure at $x > 0.7$. Upon oxidizing the samples with NaOBr solution, it is shown that the cubic perovskite structure can be extended throughout the series ($0.5 \leq x \leq 0.9$). Iodometric titrations reveal that the "as prepared" samples are fully oxygenated up to $x = 0.7$. However, the "as prepared" brownmillerite-type samples ($x = 0.8$, 0.9) show a higher degree of oxidation after chemical treatment as evidenced by PXD, electrical resistivity, magnetic susceptibility and XAS. Co K edge XAS investigated for the first time in this system shows unambiguously that there is very little change in the formal cobalt valence with increasing Sr content in the fully oxidized samples of $La_{1-x}Sr_xCoO_{3-\delta}$ ($0.5 \leq x \leq 0.9$). This result leads us to propose that there exists an internal redox equilibrium between Co(IV) and O^-: $\text{Co(IV)} + \text{O}^{2-} \leftrightarrow \text{Co(III)} + \text{O}^{-}$. This redox process is further supported by the magnetic data which shows that the effective moment reaches a maximum, and then levels off. All of the compounds show a low activation energy conductivity, probably due to impurity levels.

ACKNOWLEDGMENTS

This work was funded by the National Science Foundation Solid State Chemistry Grants DMR-93-14605 and DMR-96-13106. K.V.R. acknowledges release time awarded by Rowan University under a separately budgeted research grant. The authors thank P. Ansari and A. Aloya for help in the collection, analysis, and interpretation of the XAS data.

REFERENCES

1. J. G. Bednorz and K. A. Müller, *Z. Phys. B* **64,** 189 (1986).
2. R. von Helmolt, B. Holzapfel, L. Schultz, and K. Samwer, *Phys. Rev. Lett*. **71,** 2331 (1994).
3. S. Jin, T. H. Tiefel, M. McCormack, R. A. Fastnacht, R. Ramesh, and L. H. Chen, *Science* **264,** 413 (1994).
4. W. C. Koehler and E. O. Wollan, *J. Phys. Chem. Solids* **2,** 100 (1957).

5. J. B. Goodenough, *J. Phys. Chem. Solids* **6,** 258 (1958).
6. R. R. Heikes, R. C. Miller, and R. Mazelsky, *Physica* **30,** 1600 (1964).
7. C. S. Naiman, R. Gilmore, A. Di Bartolo, Linz, and R. Santoro, *J. Appl. Phys.* **37,** 1424 (1966).
8. G. H. Jonker, *J. Appl. Phys.* **37,** 1424 (1966).
9. P. M. Raccah and J. B. Goodenough, *Phys. Rev.* **155,** 932 (1967).
10. N. Menyuk, K. Dwight, and P. M. Raccah, *J. Phys. Chem. Solids* **28,** 549 (1967).
11. V. G. Bhide, D. S. Rajoria, G. R. Rao, and C. N. R. Rao, *Phys. Rev. B* **6,** 1021 (1972).
12. G. Thornton, B. C. Tofield, and D. E. Williams, *Solid State Commun.* **44,** 1213 (1982).
13. G. Thornton, B. C. Tofield, and A. W. Hewat, *J. Solid State Chem.* **61,** 301 (1986).
14. G. Thornton, F. C. Morrison, S. Partington, B. C. Tofield, and D. E. Williams, *J. Phys. C.: Solid State Phys.* **21,** 2871 (1988).
15. K. Asai, P. Gehring, H. Chou, and G. Shirane, *Phys. Rev. B* **40**(16), 10982 (1989).
16. V. W. Veal and D. J. Lam, *J. Appl. Phys.* **49,** 1461 (1978).
17. L. Richter, S. D. Bader, and M. B. Brodsky, *Phys. Rev. B* **22,** 3059 (1980).
18. A. F. Orchard and G. Thornton, *J. Electron Spectrosc. Relat. Phenom.* **22,** 271 (1981).
19. G. Thornton, I. W. Owen, and G. P. Diakun, *J. Phys. Condens. Matter* **3,** 417 (1991).
20. S. Masuda, M. Aoki, Y. Harada, H. Hirohashi, Y. Watanabe, Y. Sakisaka, and H. Kato, *Phys. Rev. Lett.* **71,** 4214 (1993).
21. T. Arunakavalli, G. U. Kulkarni, and C. N. R. Rao, *J. Solid State Chem.* **107,** 299 (1993).
22. M. Abbate, J. C. Fuggle, A. Fujimori, L. H. Tjeng, C. T. Chen, R. Potze, G. A. Sawatzky, H. Eisaki, and S. Uchida, *Phys. Rev. B* **47,** 16124 (1993).
23. S. R. Barman and D. D. Sarma, *Phys. Rev. B* **49,** 13979 (1994).
24. M. A. Senaris-Rodriguez and J. B. Goodenough, *J. Solid State Chem.* **116,** 224 (1995).
25. G. H. Jonker and J. H. van Santen, *Physica* **19,** 120 (1953).
26. P. M. Raccah, *J. Appl. Phys.* **39**(2), 1209 (1968).
27. J. B. Goodenough, *Mater. Res. Bull.* **6,** 967 (1971).
28. V. G. Bhide, D. S. Rajoria, C. N. R. Rao, G. Rama Rao, and V. G. Jadhan, *Phys. Rev. B* **12,** 2832 (1975).
29. C. N. R. Rao, O. M. Prakash, D. Bahadur, P. Ganguly, and S. Nagabhushana, *J. Solid State Chem.* **22,** 353 (1977).
30. H. Taguchi, M. Shimada, and M. Koizumi, *Mater. Res. Bull.* **13,** 1225 (1978).
31. D. Bahadur, S. Kollali, C. N. R. Rao, M. J. Patni, and C. M. Srivastava, *J. Phys. Chem. Solids* **40,** 981 (1979).
32. H. Taguchi, M. Shimada, and M. Koizumi, *Mater. Res. Bull.* **15,** 165 (1980).
33. A. Chaimani, M. Mathew, and D. D. Sarma, *Phys. Rev. B* **46**(16), 9976 (1992).
34. M. Itoh, I. Natori, S. Kubota, and K. Motoya, *J. Phys. Soc. Jpn.* **63,** 1486 1994.
35. K. Asai, O. Yokokura, N. Nishimori, H. Chou, J. M. Tranquada, G. Shirane, S. Higuchi, Y. Okajima, and K. Kohn, *Phys. Rev. B* **50,** 3025 (1994).
36. M. A. Senaris-Rodriguez, and J. B. Goodenough, *J. Solid State Chem.* **118,** 323 (1995).
37. A. Mineshige, M. Inaba, T. Yao, Z. Ogumi, K. Kikuchi, and M. Kawase, *J. Solid State Chem.* **121,** 423 (1996).
38. R. Mahendiran, A. K. Raychaudhuri, A. Chainini, and D. D. Sarma, *J. Phys. Condens. Matter* **7,** L561 (1995).
39. G. Briceño, H. Chang, X. Sun, P. G. Schultz, and X.-D. Xiang, *Science* **270,** 273(1995).
40. Z. L. Wang and J. Zhang, *Phys. Rev. B* **54**(2), 1155 (1996).
41. H. Watanabe and T. Takeda, Proc. Int. Conf. on Ferrites, Kyoto, 1970, p. 588. Park Press, Baltimore, MD, 1971.
42. H. Taguchi, M. Shimada, and M. Koizumi, *J. Solid State Chem.* **29,** 221 (1979).
43. I. S. Shaplygin and V. B. Lazarev, *Russ. J. Inorg. Chem.* **30**(12), 1828 (1985).
44. P. Bezdicka, A. Wattiaux, J. C. Grenier, M. Pouchard, and P. Hagenmuller, *Z. Anorg. Allg. Chem.* **619,** 7 (1993).
45. A. Nemudry, P. Rudolf, and R. Schöllhorn, *Chem. Mater.* **8,** 2232 (1996).
46. T. Guo and M. denBoer, *Phys. Rev. B* **31,** 6233 (1984).
47. See: "X-ray Absorption: Principles, Applications, Techniques of EXAFS and SEXAFS, and XANES" (D. Koningsberger and R. Reins, Eds.). Wiley, New York, 1988.
48. H. M. Rietveld, *Acta. Crystallogr.* **22,** 151 (1967).
49. H. M. Rietveld, *J. Appl. Crystallogr.* **2,** 65 (1969).
50. A. C. Larson and R. B. von Dreele, GSAS-Generalized Crystal Structure Analysis System, Los Alamos National Laboratory, Report No. LA-UR-86-748, Los Alamos, NM, 1987.
51. M. Croft, D. Sills, M. Greenblatt, C. Lee, S.-W. Cheong, K. V. Ramanujachary, and D. Tran, *Phys. Rev. B* **55**(14), 8726 (1997).
52. M. Pechini, U.S. Patent No. 3,330,697, July 1967.
53. P. Rudolf and R. Schöllhorn, *J. Chem. Soc., Chem. Commun.* **16,** 1158 (1991).
54. J. B. Thomson, A. R. Armstrong, and P. G. Bruce, *J. Am. Chem. Soc.* **118,** 11129 (1996).
55. H. Takahashi, F. Munakata, and M. Yamanaka, *Phys. Rev. B* **53**(7), 3731 (1996).
56. M. A. Korotin, S. Y. Ezhov, I. V. Solovyev, V. I. Anisimov, D. I. Khomskii, and G. A. Sawatzky, *Phys. Rev. B* **54**(8), 5309 (1996).
57. T. Saitoh, T. Mizokawa, A. Fujimori, M. Abbate, Y. Takeda, and M. Takano, *Phys. Rev. B* **55**(7), 4257 (1997).
58. R. H. Potze, G. A. Sawatzky, and M. Abbate, *Phys. Rev. B* **51**(7), 11501 (1995).
59. (a) V. I. Anisimov, J. Zaanen, and O. K. Andersen, *Phys. Rev. B* **44,** 943 (1991). (b) V. I. Anisimov, I. V. Solovyev, M. A. Korotin, M. T. Czyzyk, and G. A. Sawatzky, *Phys. Rev. B* **48,** 16129 (1993).
60. A. Sahiner, M. Croft, Z. Zhang, M. Greenblatt, I. Perez, P. Metcalf, H. Jhans, G. Liang, Y. Jeon, *Phys. Rev. B* **53**(15), 9745 (1996).
61. R. D. Shannon, *Acta Crystallogr.* **A32,** 751 (1976).